Inorg. Chem. **2006**, *45*, 1732–1738

Inorganic Chemistry
Article

Structure and Bonding in Monomeric Iron(III) Complexes with Terminal Oxo and Hydroxo Ligands

Josè Gracia Budrìa,[†] Simone Raugei,[‡] and Luigi Cavallo*[,†]

Dipartimento di Chimica, Università di Salerno, via Salvador Allende, I-84091 Baronissi (SA), Italy, and International School for Advanced Studies and INFM-DEMOCRITOS Modeling Center for Research in Atomistic Simulation, via Beirut 2−4, 34014 Trieste, Italy

Received August 11, 2005

We report on the structure and bonding in the title iron(III) complexes, containing the tris[(*N′*-*tert*-butylureayl)-*N*-ethyl]amine ligand, with density functional theory techniques. In agreement with the experimental data, a high-spin electronic state is favored for all of the systems we considered. H bonds between the terminal oxo and hydroxo ligands and NH groups present in the organic ligand coordinated to the metal have a remarkable effect on the overall coordination geometry. In fact, the structure of model complexes without H bonds shows shorter Fe–O bond lengths. This is a consequence of the ability of the H bonds to stabilize a remarkable amount of electron density localized on the terminal oxo and hydroxo ligands. Energy analysis indicates that each H bond stabilizes the nonheme complexes by roughly 35 kJ/mol. Molecular orbital analysis indicates a reduction of two Fe–O bonding electrons on going from a complex with a terminal oxo ligand to a complex with a terminal hydroxo ligand. This reduction in the number of bonding electrons is also supported by frequency analysis.

Introduction

Catalytic oxidations is a field of great importance and value because most synthetic sequences incorporate an oxidation step in one form or another. When oxidation involves transformation of organic or biochemical substrates, the catalysts of excellence usually contain activated oxygen in the form of a terminal oxo (or hydroxo) bond with a late 3d transition metal, iron and manganese in particular. Mn−O species are proposed as intermediates in biochemical systems[1] and have acquired a prominent role also in the effective and industrially relevant enantioselective epoxidation of olefins.[2,3] Fe−O species are present in many biochemical systems such as hemoglobin and cytocrome P-450.[4,5] Clearly, great efforts were dedicated to understanding the structure/function of metalloproteins, as well as to replicating their performances through the synthesis of biomimetic analogues.[6−9]

Over the years, it was well accepted that the key to understanding the stability of terminal M−O oxo and hydroxo species is the presence of multiple M−O bonds. The formation of multiple M−O bonds requires metal centers in oxidation states $\geq +4$ because high oxidation states can be associated with vacant π orbitals that can accept electron density from the terminal oxygen atom.[6] In the case of metals in oxidation states $\leq +3$, metal−oxo complexes are dominated by species containing the $M-(O)_n-M$ or $M-(OH)_n-M$ motifs.[10,11] Metalloproteins solved this problem through the presence of particular functional groups, such as carboxylates or amino acids that can act as H-bond donors, as shown by experiments on horseradish peroxidase[12] and by quantum mechanics calculations on bleomycin[13] and methane monooxygenase.[14,15] H-bond donors around the terminal ligand

---

[*] To whom correspondence should be addressed. E-mail lcavallo@unisa.it.

[†] Università di Salerno.

[‡] International School for Advanced Studies and INFM-DEMOCRITOS Modeling Center for Research in Atomistic Simulation.

(1) Su, C.; Sahlin, M.; Oliw, E. *J. Biol. Chem.* **2000**, *275*, 18830.

(2) Jacobsen, E. N. In *Comprehensive Organometallic Chemistry II*; Wilkinson, G., Stone, F. G. A., Abel, E. W., Hegedus, L. S., Eds.; Pergamon: New York, 1995; Vol. 12, Chapter 11.11.

(3) Katsuki, T. *J. Mol. Catal. A: Chem.* **1996**, *113*, 87.

(4) Springer, B. A.; Sligar, S. G.; Olsen, J. S.; Philips, G. N. *Chem. Rev.* **1994**, *94*, 699.

(5) Gerber, N. C.; Sligar, S. G. *J. Am. Chem. Soc.* **1992**, *114*, 8742.

(6) Holm, R. H. *Chem. Rev.* **1987**, *87*, 1401.

(7) Holm, R. H.; Kennepohl, P.; Solomon, E. I. *Chem. Rev.* **1996**, *96*, 2239.

(8) Holm, R. H.; Solomon, E. I. *Chem. Rev.* **2004**, *104*, 347.

(9) MacBeth, C. E.; Gupta, R.; Mitchell-Koch, K. R.; Young, V. G. J.; Lushington, G. H.; Thompson, W. H.; Hendrich, M. P.; Borovik, A. S. *J. Am. Chem. Soc.* **2004**, *126*, 2556.

(10) Kurtz, D. M., Jr. *Chem. Rev.* **1990**, *90*, 585.

(11) Pecoraro, V. L.; Baldwin, M. J.; Gelasco, A. *Chem. Rev.* **1994**, *94*, 807.

(12) Mukai, M.; Nagano, S.; Tanaka, M.; Ishimori, K.; Morishima, I.; Ogura, T.; Watanabe, Y.; Kitagawa, T. *J. Am. Chem. Soc.* **1997**, *119*, 1758.

(13) Wu, Y.-D.; Houk, K. S.; Valentine, J. S.; Nam, W. *Inorg. Chem.* **1992**, *31*, 718.

10.1021/ic051372h CCC: $33.50

Scheme 1

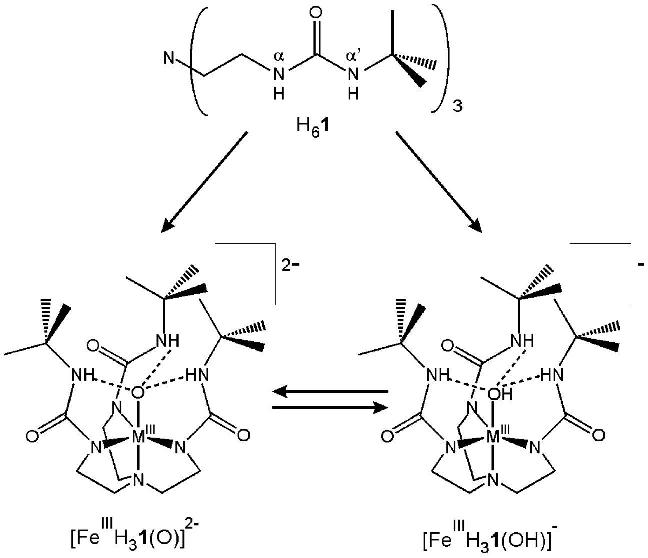

stabilize and, consequently, regulate the activity of the active site.[7,12−16]

In the case of synthetic replicas of biochemical systems, the obstacle of the poor stability of terminal M−O bonds with the metal in low oxidation states was recently overcome by the synthesis of stable Fe^{III} and Mn^{IV} complexes that present terminal metal−oxo bonds.[17] The key to stabilizing metal−oxo species with the metal in a low oxidation state was the utilization of intramolecular H bonds between the terminal oxygen atom of oxo or hydroxo groups and H-bond donors, which are present in the ligand, that complete the coordination scheme around the metal. For example, Borovik et al. describe the design, isolation, and properties for a series of mononuclear Mn,[9] Fe,[18,19] and Co[20] complexes with terminal oxo or hydroxo ligands (see Scheme 1).

The Borovik group, along with those of Masuda[21] and Berreau,[22] has developed tripodal ligands that place H-bonding groups near a metal center in monomeric complexes. The ligand tris[(*N′*-*tert*-butylureayl)-*N*-ethyl]amine ($H_6\mathbf{1}$), in Scheme 1, contains three urea groups appended from a central amine nitrogen via ethylene spacers. Deprotonation of the α-NH groups yields the anionic ligands $[H_3\mathbf{1}]^{3-}$ and $[H_2\mathbf{1}]^{4-}$, while metal ion binding is achieved through the three α-N groups and the amine nitrogen. The remaining components of the urea groups serve as scaffolding for a cavity that disposes the three α′-NH H-bond donors proximal to a fifth ligand coordinated trans to the apical amine nitrogen. This binding creates a protective H-bonding cavity around the metal center that is provided by the α′-NHR groups of the ligand. Intramolecular H bonds between the cavity α′-NH groups and the O atom coordinated to the metal center occur because thermodynamically favored six-membered rings are formed when these interactions take place. An example of this bonding scheme is the active site in oxyhemoglobin.[4] Finally, additional deprotonation of one α′-NH group of $[H_3\mathbf{1}]^{3-}$ leads to the $[H_2\mathbf{1}]^{4-}$ ligand, and the corresponding metal complexes present an intramolecular base positioned within the cavity.[18] Metal complexes of $[H_3\mathbf{1}]^{3-}$ and $[H_2\mathbf{1}]^{4-}$ have a highly anionic primary coordination sphere contained within a relatively small H-bond cavity. These properties permit M^{II} (M = Mn, Fe, Co, Zn) complexes of $[H_3\mathbf{1}]^{3-}$ and $[H_2\mathbf{1}]^{4-}$ to activate water or dioxygen and to produce monomeric M^{III}−O(H) species. Furthermore, the constrained microenvironment around the M−O(H) unit prevents the formation of $M^{III}-(n-O)_n-M^{III}$ species, the common oxidation products from Fe^{III}- and Mn^{III}-mediated dioxygen activation.

Given the relevance of these terminal oxo and hydroxo species, it is clear that soon after their synthesis great efforts were dedicated to rationalize their structure and function. Several techniques (X-ray, NMR, electron paramagnetic resonance, and electrochemical measurements) were used to characterize the structure and functional properties of these systems,[9,18,19,23] and particular interest focused on the nature of the metal−oxygen bond and on the exact role of the H bonds in their stability.[6,24−27] To contribute to the discussion, we here report on a density functional theory (DFT) study on iron complexes containing the tripodal ligands $H_6\mathbf{2}$ and $H_3\mathbf{3}$ of Chart 1. Most of the calculations involve iron species based on the $H_6\mathbf{2}$ ligand, such as $[Fe^{III}H_3\mathbf{2}(O)]^{2-}$ and $[Fe^{III}H_3\mathbf{2}(OH)]^{-}$ of Chart 1. We decided to use the $H_6\mathbf{2}$ ligand to reduce computational costs while preserving most of the basic features of the complete $H_6\mathbf{1}$ ligand. To further shed light on the role of the H bonds, we also considered systems based on the simplified $H_3\mathbf{3}$ ligand, such as $[Fe^{III}\mathbf{3}(O)]^{2-}$ and $[Fe^{III}\mathbf{3}(OH)]^{-}$ of Chart 1, which miss the three α′-NH groups that act as the H-bond donor. The most attention was focused on the nature of the Fe−O and O−H interaction, as well as on the ability of the H bonds to modulate them. Although experiments indicate that the high-spin sextet electronic state is favored,[18] we also calculated the stability of the low-spin quartet electronic state.

DFT proved to be an effective tool to investigate similar Mn- and Fe-based systems, although the correct performances of different functionals are a matter of debate.[28−44]

---

(14) Dunietz, B. D.; Beachy, M. D.; Cao, Y.; Whittington, D. A.; Lippard, S. J.; Friesner, R. A. *J. Am. Chem. Soc.* **2000**, *122*, 2828.

(15) Gherman, B. F.; Dunietz, B. D.; Whittington, D. A.; Lippard, S. J.; Friesner, R. A. *J. Am. Chem. Soc.* **2001**, *123*, 3836.

(16) Lu, Y.; Valentine, J. S. *Curr. Opin. Struct. Biol.* **1997**, *7*, 495.

(17) Borovik, A. S. *Acc. Chem. Res.* **2005**, *38*, 54.

(18) MacBeth, C. E.; Golombek, A. P.; Young, V. G. J.; Yang, C.; Kuczera, K.; Hendrich, M. P.; Borovik, A. S. *Science* **2000**, *289*, 938.

(19) MacBeth, C. E.; Hammes, B. S.; Young, V. G. J.; Borovik, A. S. *Inorg. Chem.* **2001**, *40*, 4733.

(20) Hammes, B. S.; Young, V. G. J.; Borovik, A. S. *Angew. Chem., Int. Ed.* **1999**, *38*, 666.

(21) Ogo, S.; Wada, A.; Watanabe, Y.; Iwase, M.; Wada, A.; Harata, M.; Jitsukawa, K.; Masuda, H.; Einaga, H. *Angew. Chem., int. Ed.* **1998**, *37*, 2102.

(22) Berreau, M. L.; Mahapatra, S.; Halfen, J. A.; Young, V. G. J.; Tolman, W. B. *Inorg. Chem.* **1996**, *35*, 6339.

(23) Gupta, R.; Borovik, A. S. *J. Am. Chem. Soc.* **2003**, *125*, 13234.

(24) Sheldon, R. A.; Kochi, J. *Metal-Catalyzed Oxidations of Organic Compounds*; Academic Press: New York, 1981.

(25) Nugent, W. A.; Mayer, J. M. *Metal−Ligand Multiple Bonds*; Wiley-Interscience: New York, 1988.

(26) Holm, R. H.; Donahue, J. P. *Polyhedron* **1993**, *12*, 571.

(27) Abu-Omar, M. M. *Chem. Commun.* **2003**, 2102.

(28) Salomon, O.; Reiher, M.; Hess, B. A. *J. Chem. Phys.* **2002**, *117*, 4729.

(29) Reiher, M.; Salomon, O.; Hess, B. A. *Theor. Chem. Acc.* **2001**, *107*, 48.

Chart 1

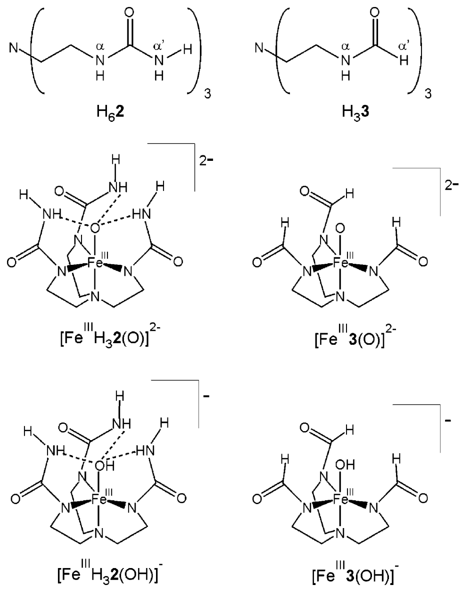

On the wake of similar papers, also in the present case, we considered the two most popular pure and hybrid functionals, namely, BP86 and B3LYP (further information can be found in the Computational Details section). A critical comparison of the results obtained with the two functionals should always be performed when investigating these kinds of systems. Nevertheless, we anticipate that in the present case the two functionals provide very similar scenarios. Thus, ambiguities that are common in other systems are not present here, and the discussion will be most focused on the chemical characterization of these systems.

Computational Details

Spin-unrestricted DFT calculations with independent treatment of the electron densities $\rho(\alpha)$ and $\rho(\beta)$ were performed on all of the systems at the GGA level with the *ADF 2004* and *Gaussian03* sets of programs.[45-47] Two popular functionals, B3LYP and BP86, were considered. B3LYP calculations utilize Becke's three-parameter hybrid exchange functional together with the correlation functional of Lee et al.[48-50] For BP86 calculations, gradient corrections were taken from the work of Becke and Perdew.[51-53] In comparisons of BP86 calculations of ADF and Gaussian, it is worth recalling that the standard implementation of this functional in the two packages is based on a different parametrization for the local potential. Within the ADF program is the potential of Vosko and co-workers,[54] whereas the Gaussian program utilizes the local potential due to Perdew.[55] Although *Gaussian03* can be set to use the Vosko potential, we preferred to use the default settings and to compare the default behavior of the two packages.

In the ADF calculations, the electronic configurations of the molecular systems were described by a triple-ζ STO basis set on iron for (3s, 3p, 3d, 4s, 4p), oxygen, nitrogen, and carbon (2s, 2p), and hydrogen (1s), augmented with single-d and p polarization functions (ADF basis set TZP).[45] The inner shells on iron (including 2p) and oxygen, nitrogen, and carbon (1s) were treated within the frozen-core approximation. In the *Gaussian03* calculations, the electronic configuration of the molecular systems was described by all-electron basis sets. For iron, we used the triple-ζ plus one polarization function basis set TZVP of Ahlrichs and co-workers,[56] while the 6-31++G(d,p) basis set[56] was used for main-group elements. A basis set with diffuse functions was considered to better capture the anionic nature of most of the compounds studied.

When spin states and $\langle S^2 \rangle$ values are talked about in the framework of DFT, a caveat is in order. For an open-shell system, with the exception of the highest spin state, it is generally not possible to exactly formulate a given spin state within DFT, and $\langle S^2 \rangle$ values are normally constructed for an approximate wave function as Slater determinants from Kohn−Sham orbitals. However, the so-obtained spin-expectation values are routinely reported in common density functional programs and are often interpreted and analyzed in applications of DFT to molecular problems. The reader is referred to the literature for an analysis of the diagnostic value of $\langle S^2 \rangle$ in Kohn−Sham DFT.[57] In this work, electronic states are characterized in terms of the spin density $S = |\rho(\alpha) - \rho(\beta)|$. Thus, an electronic state with a total spin density $S = 5$, commonly defined as a sextet, is labeled here as S5.

Finally, it is worth noting that our calculations predict a pyramidal geometry for the ureayl $-NH_2$ groups, whereas the experimental structures report a planar geometry around these groups. To investigate this point, we performed a B3LYP geometry optimization of $[Fe^{III}H_3\mathbf{2}(O)]^{2-}$, in which all of the three $-NH_2$ groups were forced to be planar. The resulting geometry is only 2 kJ/mol higher in energy relative to the fully optimized geometry. Because the two structures are substantially of the same energy, we decided to force planarity on the $-NH_2$ groups in all of the calculations that will be discussed in this paper. We made this choice to facilitate a comparison with the experimental structures.

---

(30) Lovell, T.; Han, W.-G.; Liu, T.; Noodleman, L. *J. Am. Chem. Soc.* **2002**, *124*, 5890.
(31) Lovell, T.; Liu, T.; Case, D. A.; Noodleman, L. *J. Am. Chem. Soc.* **2003**, *125*, 8377.
(32) Han, W.-G.; Lovell, T.; Liu, T.; Noodleman, L. *Inorg. Chem.* **2003**, *42*, 2751.
(33) Quinonero, D.; Musaev, D. G.; Morokuma, K. *Inorg. Chem.* **2003**, *42*, 8449.
(34) Khavrutskii, I. V.; Rahim, R. R.; Musaev, D. G.; Morokuma, K. *J. Phys. Chem. B* **2004**, *108*, 3845.
(35) Linde, C.; Åkermark, B.; Norrby, P.-O.; Svensson, M. *J. Am. Chem. Soc.* **1999**, *121*, 5083.
(36) Strassner, T.; Houk, K. N. *Org. Lett.* **1999**, *1*, 419.
(37) Ghosh, A.; Gonzalez, E.; Vangberg, T.; Taylor, P. *J. Porphyrins Phthalocyanines* **2001**, *5*, 345.
(38) Ghosh, A.; Taylor, P. *Curr. Opin. Chem. Biol.* **2003**, *7*, 113.
(39) Kumar, D.; de Visser, S. P.; Shaik, S. *J. Am. Chem. Soc.* **2004**, *126*, 5072.
(40) de Visser, S. P.; Kumar, D.; Cohen, S.; Shacham, R.; Shaik, S. *J. Am. Chem. Soc.* **2004**, *126*, 8362.
(41) Abashkin, Y. G.; Burt, S. K. *J. Phys. Chem. B* **2004**, *108*, 2708.
(42) Abashkin, Y. G.; Collins, J. R.; Burt, S. K. *Inorg. Chem.* **2001**, *40*, 4040.
(43) Cavallo, L.; Jacobsen, H. *Inorg. Chem* **2004**, *43*, 2175.
(44) Cavallo, L.; Jacobsen, H. *Angew. Chem., Int. Ed.* **2000**, *39*, 589.
(45) *ADF 2004*; Vrije Universiteit Amsterdam: Amsterdam, The Netherlands, 2004.
(46) Fonseca Guerra, C.; Snijders, J. G.; te Velde, G.; Baerends, E. J. *Theor. Chem. Acc.* **1998**, *99*, 391.
(47) Frisch, M. J.; et al. *Gaussian03*; Gaussian, Inc.: Pittsburgh, PA, 2003.
(48) Becke, A. D. *J. Chem. Phys.* **1993**, *98*, 5648.
(49) Stephens, P. J.; Devlin, F. J.; Chabalowski, C. F.; Frisch, M. J. *J. Phys. Chem.* **1994**, *98*, 11623.
(50) Lee, C.; Yang, W.; Parr, R. G. *Phys. Rev. B* **1988**, *37*, 785.
(51) Becke, A. *Phys. Rev. A* **1988**, *38*, 3098.
(52) Perdew, J. P. *Phys. Rev. B* **1986**, *33*, 8822.
(53) Perdew, J. P. *Phys. Rev. B* **1986**, *34*, 7406.
(54) Vosko, S. H.; Wilk, L.; Nusair, M. *Can. J. Phys.* **1980**, *58*, 1200.
(55) Perdew, J. P.; Zunger, A. *Phys. Rev. B* **1981**, *23*, 5048.
(56) Schaefer, A.; Horn, H.; Ahlrichs, R. *J. Chem. Phys.* **1992**, *97*, 2571.
(57) Grafenstein, J.; Cremer, D. *Mol. Phys.* **2001**, *99*, 891.

Table 1. Relative Energy, ΔE in kJ/mol, and Fe−O Bond Lengths, in Å, of the Low-Spin Quartet, S3, and High-Spin Sextet, S5, Electronic States of Several Fe−O Systems

		low spin		high spin	
system	method	ΔE	Fe−O	ΔE	Fe−O
$[Fe^{III}O]^+$	BP86-ADF	53	1.611	0	1.638
	BP86-G03	45	1.568	0	1.639
	B3LYP	21	1.701	0	1.642
$[Fe^{III}(OH)]^{2+}$	BP86-ADF	89	1.848	0	1.718
	BP86-G03	98	1.792	0	1.726
	B3LYP	53	1.956	0	1.715
$[Fe^{III}H_3\mathbf{2}(O)]^{2-}$	BP86-ADF	31	1.774	0	1.803
	B3LYP	63	1.745	0	1.781
$[Fe^{III}H_3\mathbf{2}(OH)]^-$	BP86-ADF	4	1.886	0	1.962
	B3LYP	41	1.870	0	1.952

Results and Discussion

Model FeO Compounds. We begin this section with a discussion of the small $[Fe^{III}O]^+$ and $[Fe^{III}(OH)]^{2+}$ molecules. The electronic structure and the bonding scheme in these systems will be used as models for the corresponding properties in the more complex nonheme systems discussed below. In the following, the quartet and sextet electronic states will be labeled S3 and S5, respectively, from the total spin densities $S = 3$ and 5, respectively; see the Computational Details section.

The energy data reported in Table 1 show that for both systems the high-spin sextet electronic state S5 is clearly favored over the low-spin quartet electronic state S3 with either the pure or hybrid functionals. For $[Fe^{III}O]^+$, this finding is supported by experimental data,[58] and it is in good accordance with more accurate CCSD(T) values that predicted the high-spin S5 state to be favored by 52 kJ/mol relative to the low-spin S3 state[59] and with other calculations at different levels of theory.[60,61] Although $[Fe^{III}(OH)]^{2+}$ was investigated less, also in this case, the literature indicates that a high-spin sextet configuration is favored.[62] From a geometric viewpoint, in the favored S5 geometry of $[Fe^{III}O]^+$ and $[Fe^{III}(OH)]^{2+}$, the pure and hybrid functionals perform very similarly, and both predict that the Fe−O bond in $[Fe^{III}O]^+$ is roughly 0.08 Å shorter than that in $[Fe^{III}(OH)]^{2+}$; see Table 1. In agreement with previous results, both pure and hybrid functionals predict a linear geometry for $[Fe^{III}(OH)]^{2+}$.[59] This differs from neutral and monocationic monohydroxides, which result in bent geometries with an Fe−O−H angle of about 140°.[63] Finally, the ADF and Gaussian03 BP86 results are in good agreement in terms of both energy and geometry. This implies that B3LYP-G03 and BP86-ADF calculations on these iron systems can be compared consistently.

In agreement with previous studies,[64] natural bond order (NBO) analysis on the high-spin S5 B3LYP geometry of $[Fe^{III}O]^+$, summarized in Table 2, indicates the presence of four bonding electrons between the Fe and O atoms. Two of them are paired to form a classical σ bond, while the other two electrons are unpaired and are localized in π-bonding orbitals. As was already noticed, the bonding scheme in $[Fe^{III}O]^+$ is analogous to that in the ground state of O_2.[64] Perfect electron pairing in $[Fe^{III}O]^+$ suffers from repulsion between the π electrons. To avoid this energetically demanding interaction, $[Fe^{III}O]^+$ trades perfect pairing for a more favorable high-spin S5 configuration. The presence of four bonding electrons supports the idea that the Fe−O interaction has the character of a double bond. In terms of NBO analysis, the Wiberg bond index, WBI, of the Fe−O bond is 1.08.

A similar analysis on the high-spin S5 B3LYP geometry of $[Fe^{III}(OH)]^{2+}$ indicates the presence of only two Fe−O bonding electrons. They are unpaired and are both located in π-type orbitals. The presence of two bonding electrons supports the idea that the Fe and O interaction in $[Fe^{III}(OH)]^{2+}$ has the character of a single bond. While the Fe−O π-bonding scheme in $[Fe^{III}(OH)]^{2+}$ is very similar to that in $[Fe^{III}O]^+$, we remark that the NBO analysis indicates the presence of no σ-bonding electrons in $[Fe^{III}(OH)]^{2+}$. The reduced number of bonding electrons between the Fe and O atoms is also confirmed by the remarkably smaller WBI for Fe−O in $[Fe^{III}(OH)]^{2+}$, 0.67, which is 0.41 lower than that in $[Fe^{III}O]^+$. Of course, NBO analysis indicates the presence of a classical σ bond between the O and H atoms, which replaces the σ Fe−O bond in the parent compound $[Fe^{III}O]^+$, with a WBI of 0.58. Finally, because the Fe−O−H moiety is not linear in the nonheme complexes that we will discuss in the following, we also analyzed the S5 B3LYP bent geometry of $[Fe^{III}(OH)]^{2+}$, in which the Fe−O−H angle is fixed at 110° (roughly the value we calculated for this angle in the nonheme complexes discussed in the following). In this bent geometry, the Fe−O bond is 0.155 Å longer than that in the linear geometry, and the NBO analysis results in a bonding scheme between the Fe and O atoms very similar to that of the linear geometry.

Structures and Energetics of Nonheme Systems. We focus now on the nonheme $[Fe^{III}H_3\mathbf{2}(O)]^{2-}$ and $[Fe^{III}H_3\mathbf{2}(OH)]^-$ species, for which experimental data are available. For the former system, both the pure and hybrid functionals clearly predict that the high-spin S5 electronic state is favored, with the low-spin S3 electronic state at least 30 kJ/mol higher in energy; see Table 1. For the latter system, the S5 state is also favored by both functionals. However, the energy gap between the two states is considerably reduced, and in the case of the pure functional, the preference for the S5 state is rather small. We recall here that the tendency of pure DFT approaches to systematically favor low-spin states is well documented in the literature.[28,29,34,38,65−67] Nevertheless, in the present case, both the pure and hybrid DFT predictions

---

(58) Husband, J.; Aguirre, F.; Ferguson, P.; Metz, R. *J. Chem. Phys.* **1999**, *111*, 1433.

(59) Irigoras, A.; Fowler, J. E.; Ugalde, J. M. *J. Am. Chem. Soc.* **1999**, *121*, 8549.

(60) Fiedler, A.; Hrusak, J.; Koch, W.; Schwarz, H. *Chem. Phys. Lett.* **1993**, *211*, 242.

(61) Filatov, M.; Shaik, S. J. *Phys. Chem. A* **1998**, *102*, 3835.

(62) Schröder, D.; Bärsch, S.; Schwarz, H. *J. Phys. Chem. A* **2000**, *104*, 5101.

(63) Trachtman, M.; Markham, G. D.; Glusker, J. P.; George, P.; Bock, C. W. *Inorg. Chem.* **2001**, *40*, 4230.

(64) Fiedler, A.; Schroeder, D.; Shaik, S.; Schwarz, H. *J. Am. Chem. Soc.* **1994**, *116*, 10734.

(65) Khavrutskii, I. V.; Musaev, D. G.; Morokuma, K. *J. Am. Chem. Soc.* **2003**, *125*, 13879.

(66) Cavallo, L.; Jacobsen, H. **2003**, 892.

(67) Cavallo, L.; Jacobsen, H. *J. Phys. Chem. A* **2003**, *107*, 5466.

Table 2. Relevant Data from the NBO Analysis of the Most Stable Electronic States As Obtained from the Unrestricted B3LYP Calculations

	occupation of bonding MO[a]		NPA charge[b]				spin population (% of spin density)			
system	σ	π	Fe	O	WBI[c] for Fe−O	spin density[d] $\alpha-\beta$	Fe	O(H)	ligand	Fe−O frequency, cm^{-1}
$[Fe^{III}O]^{+}$	2	1, 1	1.45	−0.45	1.08	5	3.8 (76)	1.2 (24)	0.0 (0)	832
$[Fe^{III}(OH)]^{2+}$	0	1, 1	1.98	−0.62	0.67	5	3.9 (79)	1.0 (20)	0.1 (1)	740
$[Fe^{III}H_3\mathbf{2}(O)]^{2-}$	1	1, 1	1.68	−1.19	0.54	5	3.9 (79)	0.6 (12)	0.5 (9)	697
$[Fe^{III}H_3\mathbf{2}(OH)]^{-}$	0	1	1.76	−1.20	0.24	5	4.0 (80)	0.2 (4)	0.8 (16)	473
$[Fe^{IV}H_3\mathbf{2}(O)]^{-}$	2	1, 1	1.46	−0.76	0.97	4	3.0 (75)	0.5 (12)	0.5 (13)	855
$[Fe^{III}H_2\mathbf{2}(OH)]^{2-}$	0	1	1.74	−1.19	0.32	5	4.1 (81)	0.3 (6)	0.6 (13)	522
$[Fe^{IV}H_2\mathbf{2}(O)]^{2-}$	2	1, 1	1.42	−0.68	1.03	4	2.9 (72)	0.5 (13)	0.6 (15)	868
$[Fe^{III}\mathbf{3}(O)]^{2-}$	0	1, 1	1.60	−1.08	0.70	5	4.0 (81)	0.7 (15)	0.3 (4)	773
$[Fe^{III}\mathbf{3}(OH)]^{-}$	0	1	1.76	−1.13	0.34	5	4.2 (84)	0.2 (5)	0.6 (11)	585
$[Fe^{IV}\mathbf{3}(O)]^{-}$	2	1, 1	1.40	−0.59	1.10	4	3.1 (77)	0.6 (14)	0.3 (9)	910

[a] Occupation of σ- and π-bonding molecular orbitals (MOs). For instance, 2 and 1, 1 for $[Fe^{III}O]^{+}$ means that NBO analysis indicates the presence of a doubly occupied σ-bonding MO and of two singly occupied π-bonding MOs. [b] NPA = natural population analysis. [c] WBI = Wiberg bond index. [d] Total spin density ($\alpha-\beta$ electrons) of the system.

are in good qualitative agreement with the high-spin electronic state determined experimentally.[9,18]

Computed geometries of the two high-spin S5 systems reveal the metal in a trigonal-bipyramid coordination environment, in the cavity provided by the $[H_3\mathbf{2}]^{3-}$ ligand. The three deprotonated N atoms, N_{eq}, define the equatorial plane, while the amine N atom, N_{ax}, and the O atom bound to Fe are aligned on the axis of the bipyramid. As is common in M−O species,[6] we found the Fe atom to be slightly pulled out of the equatorial plane toward the O atom. The value calculated for $[Fe^{III}H_3\mathbf{2}(O)]^{2-}$, 0.51 Å, is in good agreement with the experimental value of 0.41 Å. In both systems, the urea arms are nearly perpendicular to the equatorial plane. In the case of $[Fe^{III}H_3\mathbf{2}(O)]^{2-}$, the three protonated N atoms are oriented in such a way as to project one of the H atoms toward the M−O unit to form three H bonds with the oxo ligand, and the overall complex assumes an almost perfect C_3 symmetry. Instead, in the case of $[Fe^{III}H_3\mathbf{2}(OH)]^{-}$, the hydroxyl O−H bond prevents the system from assuming a C_3 symmetry. The O−H bond points between two protonated N atoms, which are consequently forced to bend back toward the third protonated N atoms, the one trans to the O−H bond. Thus, the system assumes a distorted C_s symmetry, with the Fe−O−H bond in the (almost) symmetry plane. The hydroxyl O atom forms H bonds with the three NH_2 groups, although distances are quite different. The shortest N−H···O distance occurs with the NH_2 group trans to the O−H bond.

The calculated lengths of the Fe−O and Fe−N_{eq} bonds in both systems are in excellent agreement with the experimental values, with a deviation of roughly 0.05 Å, independent of the specific functional used. Differently, the Fe−N_{ax} bond length is overestimated by roughly 0.15−0.20 Å in both systems and by both functionals. To investigate in more detail this point, we performed a B3LYP geometry optimization of $[FeH_3\mathbf{2}(O)]^{2-}$, in which the Fe−$N_{ax}$ distance was fixed to the experimental value. The resulting geometry is only 5 kJ/mol higher in energy relative to the fully optimized geometry of Figure 1. This very small energy difference indicates that the stretching of the Fe−N_{ax} bond is rather soft. It is rather difficult to rationalize this discrepancy between the calculated and experimental values.

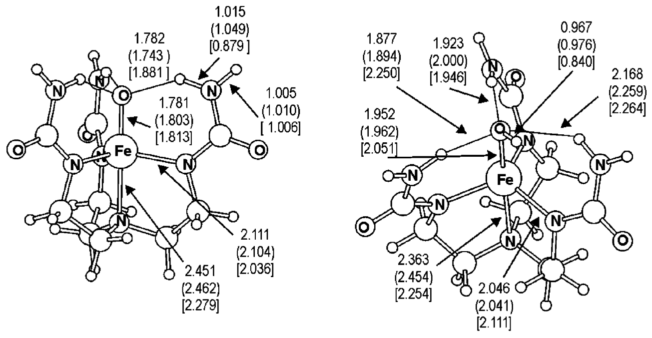

$[Fe^{III}H_3\mathbf{2}(O)]^{2-}$ $[Fe^{III}H_3\mathbf{2}(OH)]^{-}$

Figure 1. High-spin S5 B3LYP geometries of $[FeH_3\mathbf{2}(O)]^{2-}$ and $[FeH_3\mathbf{2}(OH)]^{-}$. Distances in parentheses are those obtained for the S5 BP86 (ADF) geometry, while the values in square brackets refer to the X-ray geometry. All distances are in angstroms.

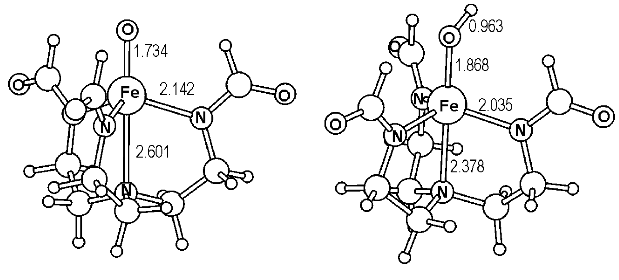

$[Fe^{III}\mathbf{3}(O)]^{2-}$ $[Fe^{III}\mathbf{3}(OH)]^{-}$

Figure 2. High-spin S5 B3LYP geometry of $[Fe^{III}\mathbf{3}(O)]^{2-}$ and $[Fe^{III}\mathbf{3}(OH)]^{-}$. Distances are in angstroms.

It might be due to a weakness of the computations as well as to packing effects or to the presence of the cations in the solid state. However, because all of the remaining geometrical parameters were substantially unaffected by the presence of this constraint, we believe that the poor prediction of the Fe−N_{ax} bond is of scarce relevance.

Role of the H Bonds. To test for the influence of the N−H···O H bonds on the overall geometry, we performed a B3LYP geometry optimization of $[Fe^{III}\mathbf{3}(O)]^{2-}$ in the high-spin S5 electronic state; see Figure 2. The absence of the H bonds has a remarkable effect on the overall geometry. The Fe atom is slightly pulled away from the equatorial plane defined by the N_{ax} atoms because it is 0.62 Å out of the plane. The Fe−O bond shrinks by 0.05 Å, while the Fe−

N_{eq} and Fe−N_{ax} bonds elongate by 0.03 and 0.15 Å, respectively. Natural population analysis, NPA, charges probably hold an explanation for these changes in the Fe bonds. In fact, the NPA charge of the O atom in $[Fe^{III}\mathbf{3}(O)]^{2-}$, −1.08e, is smaller than that in $[Fe^{III}H_3\mathbf{2}(O)]^{2-}$, −1.19e (see Table 2), and more electron density is localized on the Fe atom, which has a NPA charge of 1.60e in $[Fe^{III}\mathbf{3}(O)]^{2-}$. The less electron-deficient metal atom results in longer Fe−N distances.

With regards to the three equivalent N−H···O H bonds in the high-spin S5 $[Fe^{III}H_3\mathbf{2}(O)]^{2-}$, the WBI for each of them, 0.08, is considerably greater than the WBI predicted at the same level of theory for the H bond in the water dimer, 0.03. NBO analysis indicates rather strong H bonds also in $[Fe^{III}H_3\mathbf{2}(OH)]^{-}$, although two of them are shorter than the third. To have an energy estimation of the stabilization due to the presence of the H bonds, we calculated the energy of the reaction

$$[Fe^{III}H_3\mathbf{2}]^{2-} + [Fe^{III}\mathbf{3}(O)]^{2-} \rightarrow [Fe^{III}H_3\mathbf{2}(O)]^{2-} + [Fe^{III}\mathbf{3}]^{2-} \quad (1)$$

This reaction corresponds to the exchange of the O ligand from a system that cannot form H bonds, $[Fe^{III}\mathbf{3}(O)]^{2-}$, to a system that is stabilized by H bonds, $[Fe^{III}H_3\mathbf{2}(O)]^{2-}$. Considering that the two systems are characterized by very similar Fe−ligand bonds, any energy preference for the right side of eq 1 can be correlated to additional stability because of the presence of the H bonds in $[Fe^{III}H_3\mathbf{2}(O)]^{2-}$. The right side of eq 1 is favored by 109 kJ/mol. Considering that three H bonds are formed on going from $[Fe^{III}\mathbf{3}(O)]^{2-}$ to $[Fe^{III}H_3\mathbf{2}(O)]^{2-}$, this means that each H bond stabilizes $[Fe^{III}H_3\mathbf{1}(O)]^{2-}$ by roughly 35 kJ/mol. The remarkably strong H bonds that we predicted support the commonly accepted idea that they are the key to understanding the stability of these systems.

Fe−O Bonding in Nonheme Systems. NBO analysis on the high-spin S5 $[Fe^{III}H_3\mathbf{2}(O)]^{2-}$ system indicates the presence of one σ-bond electron and two unpaired π-bonding electrons between the Fe and O atoms. The bonding Fe−O NBO orbitals for S5 $[Fe^{III}H_3\mathbf{2}(O)]^{2-}$ are reported in Figure 3. Visual inspection confirms the σ and π nature of the orbitals and indicates a good Fe contribution to all of the Fe−O bonds. Using the NBO analysis of S5 $[Fe^{III}O]^{+}$ as a model, there is the reduction of one σ-bonding electron. The reduction of one Fe−O bonding electron occurs also when comparing S5 $[Fe^{III}H_3\mathbf{2}(OH)]^{-}$ with S5 $[Fe^{III}(OH)]^{2+}$, in this case, one of the two unpaired π electrons. Oxidation of Fe from +3 to +4, as in S4 $[Fe^{IV}H_3\mathbf{2}(O)]^{-}$, restores the two Fe−O σ-bonding electrons, despite the H bonds between the $[H_3\mathbf{2}]^{3-}$ frame and the terminal oxo ligand.

NBO analysis gives a particular point of view of the Fe−O bonding characteristics in terms of σ- and π-bonding electrons. Iron(IV) systems with terminal oxo ligands show multiple M−O bond characteristics (two σ and two π electrons). In full agreement with known ideas, the number and type of bonding electrons are independent of the environment around the Fe−O bond. Conversely, for iron(III) systems, the ligands show a clear influence. In the $[Fe^{III}\mathbf{3}(O)]^{2-}$ system model, there are no σ-bonding electrons, in agreement with the fact that multiple Fe−O bonds require metals in the high oxidation state. Instead, in the $[Fe^{III}H_3\mathbf{2}(O)]^{2-}$ system, there is one additional σ-bonding electron, a consequence of the H bonds that involve the terminal oxo ligand and that deplete the electron density from the metal.

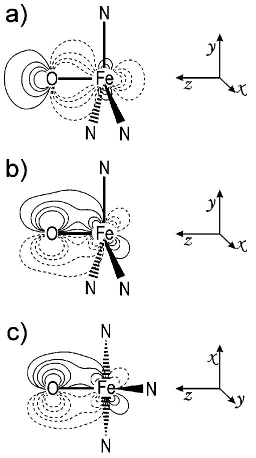

Figure 3. Plots of the σ (part a) and π (parts b and c) Fe−O bonding orbitals of the high-spin S5 $[Fe^{III}H_3\mathbf{2}(O)]^{2-}$ system as derived from NBO analysis.

Consistent with the previous discussion, for both of the high-spin S5 $[Fe^{III}H_3\mathbf{2}(O)]^{2-}$ and $[Fe^{III}H_3\mathbf{2}(OH)]^{-}$ systems, the reduction in the number of bonding electrons results in a decrease of the WBI of the Fe−O bond of roughly 0.5 relative to the model compounds $[Fe^{III}O]^{+}$ and $[Fe^{III}(OH)]^{2+}$, while the Fe−O WBI in $[Fe^{IV}H_3\mathbf{2}(O)]^{-}$ is rather similar to that in $[Fe^{III}O]^{+}$ (see Table 2).

With regards to spin densities, it is substantially localized (roughly 75−80%) on the Fe atom in most of the complexes reported in Table 2, while the O atom and the ligand usually bear only 10−15% of the spin density. The Fe/O spin partitioning ratio in the nonheme systems with H bonds and with a terminal oxo ligand is roughly 6, while in the analogous systems with a terminal hydroxo ligand, it is remarkably higher, >10. This indicates that a terminal oxo ligand is much more able than a univalent hydroxo ligand to delocalize the spin density away from the metal center. This finding is in agreement with the previous results of Ghosh and co-workers on $Fe^{IV}(porphyrinato)(OCH_3)_2$ and $[(bipyridyl)_4Fe_2(\mu\text{-}O)_2)]$ complexes.[68,69] As pointed out by Ghosh and co-workers, while localization of the spin density is a feature of interest, it is difficult to extrapolate possible effects in terms of reactivity.[68]

Frequency Analysis. A similar trend in the Fe−O bond strength can be derived from frequency analysis that resulted in the values for the Fe−O stretching mode reported in Table 2. We first note that the frequency we calculated for the Fe−O stretching in S5 $[Fe^{III}H_3\mathbf{2}(O)]^{2-}$, 697 cm^{-1}, is in very good agreement with the experimental value of 671 cm^{-1}.[9] The frequency of the Fe−O vibration in S5 $[Fe^{III}H_3\mathbf{2}(O)]^{2-}$

---

(68) Conradie, J.; Swarts, J. C.; Ghosh, A. *J. Phys. Chem. B* **2004**, *108*, 452.

(69) Ghosh, A.; Tangen, E.; Gonzalez, E.; Que, L., Jr. *Angew. Chem., Int. Ed.* **2004**, *43*, 834.

Scheme 2

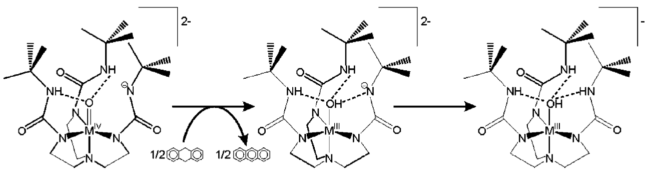

is 76 cm^{-1} lower than that in S5 [Fe^{III}**3**(O)]$^{2-}$, which again remarks the effect of the H bonds on the strength of the Fe−O bond, and it is remarkably greater, by 224 cm^{-1}, than that in S5 [Fe^{III}H$_3$**2**(OH)]$^-$. The values for the Fe−O vibration that we calculated for S5 [Fe^{III}O]$^+$ and S4 [Fe^{IV}H$_3$**2**(O)]$^-$, around 850 cm^{-1}, are in the same range of the experimental Fe−O stretching frequency of a monomeric Fe^{IV}−O complex, 834 cm^{-1}.[70] This again supports the Fe−O bonding scheme that we derived on the basis of NBO analysis. Finally, it is worth noting that the WBI and the values of the Fe−O stretching reported in Table 2 substantially parallel each other, indicating the following order in the Fe−O bond strength: [Fe^{III}O]$^+$ ≈ [Fe^{IV}H$_3$**2**(O)]$^-$ ≈ [Fe^{III}**3**(O)]$^{2-}$ > [Fe^{III}(OH)]$^{2+}$ ≈ [Fe^{III}H$_3$**2**(O)]$^{2-}$ > [Fe^{III}H$_3$**2**(OH)]$^-$.

Formation of Nonheme Complexes. In this final section, we report on the energetics associated with [FeH$_3$**2**(OH)]$^-$ formation. According to Borovik and co-workers, a possible reaction path that starts from a monomeric Fe^{IV} species is depicted in Scheme 2.[18]

To evaluate the energy changes associated with the structures of scheme 2, we optimized the geometries of S4 [Fe^{IV}H$_2$**2**(O)]$^{2-}$ and S5 [Fe^{III}H$_2$**2**(OH)]$^{2-}$, reported in Figure 4. The main structural feature of S4 [Fe^{IV}H$_2$**2**(O)]$^{2-}$ is the rather short bond between the Fe atom and the N$_{eq}$ atom of the arm that bears the deprotonated N atom. This can be easily explained considering that the corresponding ureaylate group is strongly desymmetrized by the presence of a local charge on the terminal N atom, which results in long and short C−N$_{eq}$ and C−N terminal bonds relative to the other two protonated ureayl groups. Charge accumulation on the N$_{eq}$ atom leads to a short Fe−N$_{eq}$ bond. The strong O−H···N H bond in [Fe^{III}H$_2$**2**(OH)]$^{2-}$ partially alleviates this behavior.

Both steps of Scheme 2 are exoergonic, the former by 207 kJ/mol. This indicates that, as was already suggested by Borovik and co-workers, the Fe^{IV}═O species has a strong thermodynamic driving force to form an Fe^{III}−OH complex.[9] The second step is favored by 29 kJ/mol only. Incidentally, the relative stability that we calculated for S5 [Fe^{III}H$_2$**2**(OH)]$^{2-}$ and S5 [Fe^{III}H$_3$**2**(O)]$^{2-}$ is exactly the value calculated by Borovik and co-workers with a slightly different approach.[9]

Conclusions

In this paper, we reported on the structure and bonding of nonheme iron complexes. The main conclusions can be summarized as follows:

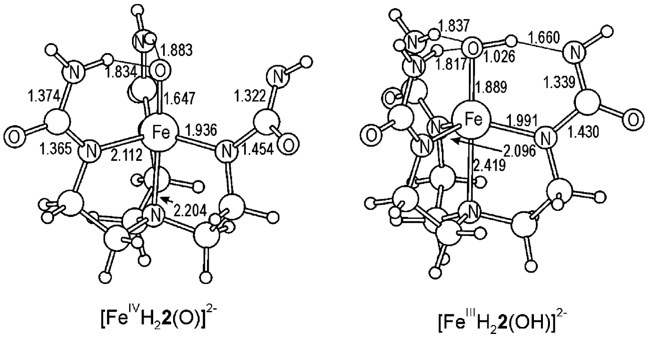

Figure 4. B3LYP geometries of the high-spin S4 [Fe^{IV}H$_2$**2**(O)]$^{2-}$ and S5 [Fe^{III}H$_2$**2**(OH)]$^{2-}$ systems. Distances are in angstroms.

(1) Computed geometries are in rather good agreement with the X-ray structures. Moreover, in agreement with the experimental data, the high-spin S5 electronic state is favored for all of the systems that we considered. These results validate the computational approach that we used.

(2) The H bonds have a remarkable effect on the overall coordination geometry. In fact, the structure of model complexes without H bonds shows shorter Fe−O and longer Fe−N bond lengths relative to the corresponding structures in the presence of the H bonds. NPA charges suggest that this is a consequence of the ability of the H bonds to stabilize a remarkable amount of electron density localized on the terminal O and OH ligands. Energy analysis indicates that each H bond stabilizes the nonheme complexes by roughly 35 kJ/mol.

(3) NBO analysis indicates the presence of three bonding electrons (one σ and two unpaired π) in S5 [Fe^{III}H$_3$**2**(O)]$^{2-}$ and of only one π-bonding electron in S5 [Fe^{III}H$_3$**2**(OH)]$^-$. A similar reduction of two bonding electrons on going from a complex with an O ligand to a complex with an OH ligand is calculated for the parent high-spin Fe^{III}O$^+$ and Fe^{III}(OH)$^{2+}$ complexes. The different numbers of bonding electrons are also indicated by the much higher frequency calculated for the Fe−O stretching in S5 [Fe^{III}H$_3$**2**(O)]$^{2-}$ relative to S5 [Fe^{III}H$_3$**2**(OH)]$^-$.

(4) Our analysis on the energetics of the reaction connected to the formation of the nonheme complexes supports the suggestion of Borovik and co-workers that Fe^{IV}═O species have a strong thermodynamic driving force to form an Fe^{III}−OH complex.

Finally, we remark that our results do not depend on the specific density functional approach used and that hybrid and pure functionals provide a similar scenario. As usual, the only difference between the two families of functionals is the tendency of pure functionals to overestimate the stability of low-spin states relative to hybrid functionals.

Acknowledgment. We thank Prof. Tom K. Woo (University of Western Ontario) and the SHARCNET project for generous access to computer resources and the University of Salerno (Grant Medie Apparecchiature 2002) for financial support.

Supporting Information Available: Cartesian coordinates and energies of all of the species discussed in the paper and complete ref 47. This material is available free of charge via the Internet at http://pubs.acs.org.

IC051372H

---

[70] Rohde, J.-U.; In, J.-H.; Lim, M. H.; Brennessel, W. W.; Bukowski, M. R.; Stubna, A.; Münck, E.; Nam, W.; Que, L., Jr. *Science* **2003**, *299*, 1037.